ISSN: 2414-1895 DOI: 10.6919/ICJE.202405_10(5).0023

Research on the Welding Performance of 0Cr13Ni4Mo Martensitic Stainless Steel for Turbine Runners

Zhongmei Zuo[1], Qing Qin[1], Xinyu Zhou[2], Daocheng Luan[2,*]

[1] Chengdu Jincheng College, Chengdu 611731, China

[2] College of Materials, Xihua University, Chengdu 610039, China

Abstract

The welding performance of 0Cr13Ni4Mo martensitic stainless steel for water turbine runners was studied at different welding temperatures. The microstructure of the weld was analysed by optical microscope, XRD, SEM, etc. The mechanical properties of impact toughness and tensile strength of the welded zone was tested. The results show that the shielded flux of 0Cr13Ni4Mo martensitic stainless steel was well formed, and the flaw detection was qualified. The welding temperature has little effect on the microstructure of the welded joint. The microstructure of the weld under different welding parameters is mainly lath martensite. The tensile strength, impact toughness and the plasticity of the weld exhibited the best performance at a welding temperature of 170 ℃ and with a line energy of 13 kJ/cm. The tensile strength of the welded joint is higher than 812 MPa, and the impact work is 49 J.

Keywords

Martensitic Stainless Steel; Welding Process; Lath Martensite; Water Turbine; Mechanical Properties.

1. Introduction

The main equipment of hydropower generation is the water turbine, with the runner being its core component [1]. Typically, the runner is composed of blade, upper canopy, and lower ring, which are welded together. Therefore, welding as the dominant thermal processing method in the manufacture and repair of the runner, its quality affects the normal operation and service life of the water turbine significantly. The key project undertaken in the Yangtze River basin involves the construction of domestically developed 800-1000MW ultra-large hydroelectric station [2].

The runner is typically made of cast 0Cr13Ni4Mo martensitic stainless steel. The casting process, heat treatment process and mechanical properties of 0Cr13Ni4Mo martensitic stainless steel have been deeply studied domestically and abroad. However, the research on its welding process and the performance of weld is relatively limited [3]. Particularly, the welding of martensitic stainless steel for 800-1000MW ultra large water turbine runner has not been carried out at present. In order to ensure the safe operation and even excellent performance of large water turbine components, they need to be repaired by welding where the flowing water mixed with sediment caused erosion, and then wear and tear during actual service. Therefore, the research on the welding performance of 0Cr13Ni4Mo martensitic stainless steel has significant scientific and practical value.

In order to study the performance of welded joints of 0Cr13Ni4Mo martensitic stainless steel, the optimal welding process was selected. The plate joint welding test is designed to study the effects of welding current and multi-pass welding interlayer temperature on the microstructure of the welded joints. This research focused on the influence of welding interlayer temperature on the welding characteristics of 0Cr13Ni4Mo martensitic stainless steel.

ISSN: 2414-1895 DOI: 10.6919/ICJE.202405_10(5).0023

2. Test Materials and Process

2.1 Test Materials

The experiment uses ZG0Cr13Ni4Mo martensitic stainless-steel plate with a dimension of 150×150×20 mm^3, and its chemical composition is shown in Table.1. According to the standard GB/T4237-2015, the heat treatment process involves a two-step solid solution treatment (1040℃+1010℃) and a two-step tempering (620℃+600℃). The mechanical properties of the as-casting state are shown in Table.2.

Table 1. Chemical composition (%) of ZG0Cr13Ni4Mo martensitic stainless steel

element	C	Si	Mn	P	S	Cr	Ni	Mo
content	0.032	0.28	0.71	0.019	0.002	12.45	4.47	0.52
standard specified value	0.04	0.6	1.00	0.028	0.008	12.0-13.5	3.8-5.0	0.4-1.0

Table 2. Mechanical properties of ZG0Cr13Ni4Mo martensitic stainless steel

yield strength $R_{P0.2}$/MPa	tensile strength Rm/MPa	Elongation A/%	section shrinkage rate Z/%	impact toughness(0℃) AkV_2/J	bend 180° (d=4a)	hardness HBW
580	780	20	55	100	qualified	220-285

The stainless-steel welding rod in this test is E410NiMo-15 type (0Cr13Ni4Mo), which is produced by Zhengzhou Research Institute of Mechanical Engineering Co., Ltd. Its main components are shown in Table.3. The diameter of the welding rod is φ4 mm, which is consistent with the requirement as described in the standard GB/T 983-2012.

Table 3. Chemical composition of E410NiMo-15 stainless-steel welding rod (%)

element	C	Si	Mn	P	S	Cr	Ni	Mo
content	0.037	0.45	0.80	0.025	0.010	12.32	4.17	0.62
standard specified value	0.06	0.90	1.00	0.04	0.03	11.0-12.5	4.0-5.0	0.40-0.70

2.2 Welding Tests

The various welding tests were conducted by using the IGBT inverter rectifier arc welding machine. The welding plate used 0Cr13Ni4Mo low-hydrogen welding rod with the same quality as the base material. The welding bevel form used a V-type (angle is 60 °) for both single-sided welding and double-sided forming, as shown in Fig.1. The welding rod used in the test was alkaline low-hydrogen welding rod, with a diameter of φ4 mm. Direct current reverse polarity was applied, and the welding current is 160 A. The infrared thermometer was used to measure the temperature of each layer of weld channel. The interlayer temperature of each welding layer need to be controlled, which was set as 140 ℃, 170 ℃, and 200 ℃, respectively. The parameters of the plate joint welding process is detailed in Table.4. Before welding, the rod was dried for 1.5 h at 300 ℃ by using a far-infrared high-low temperature welding rod oven (YZH2-30KG) with a TI120 series infrared thermometer. The preheating temperature of the welding test plate was 140 ℃.

ISSN: 2414-1895 DOI: 10.6919/ICJE.202405_10(5).0023

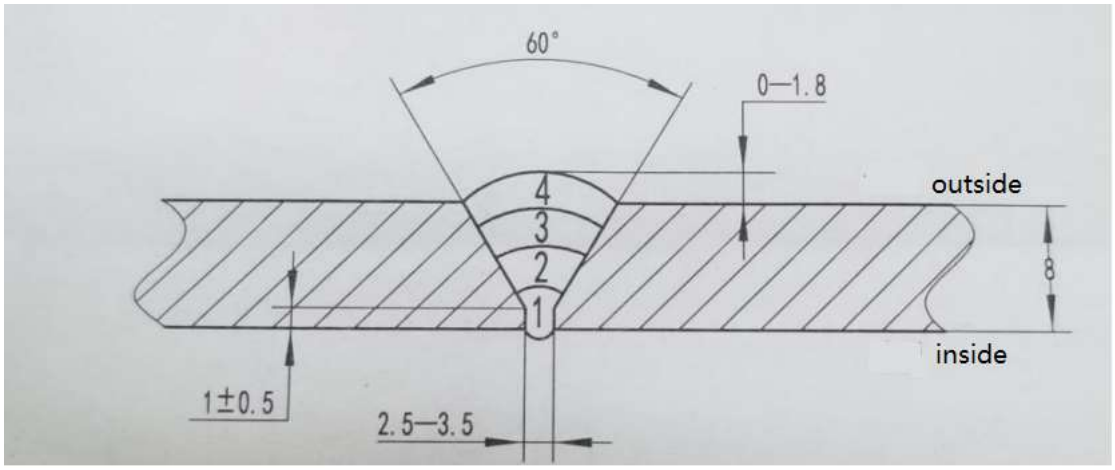

Fig.1 design diagram of experimental crevasse

Table 4. Process parameters of plate joint welding

sample number	preheating temperature (℃)	welding current (A)	interlayer temperature (℃)	line energy (kJ/cm)
1#	140	160	140	13
2#	140	160	170	13
3#	140	160	200	13

Etching of the weld was applied before microstructure analysis. The solution of etchant used 10 g of solid ferric chloride and 40 ml of hydrochloric acid which was diluted to 100 ml. The microstructure was observed on the OLYMPUS GX-71F metallographic microscope. The DX-2500 X-ray diffraction (XRD) analyser was used for phase analysis of the welded joints (mainly seam and heat-affected zone) under different welding process parameters. Cu target was selected. The accelerating voltage and accelerating current were 30kV and 10mA, respectively. The scanning step was 0.01 °/S, and the scanning angle was 20°-120°.

2.3 Tests of Mechanical Properties

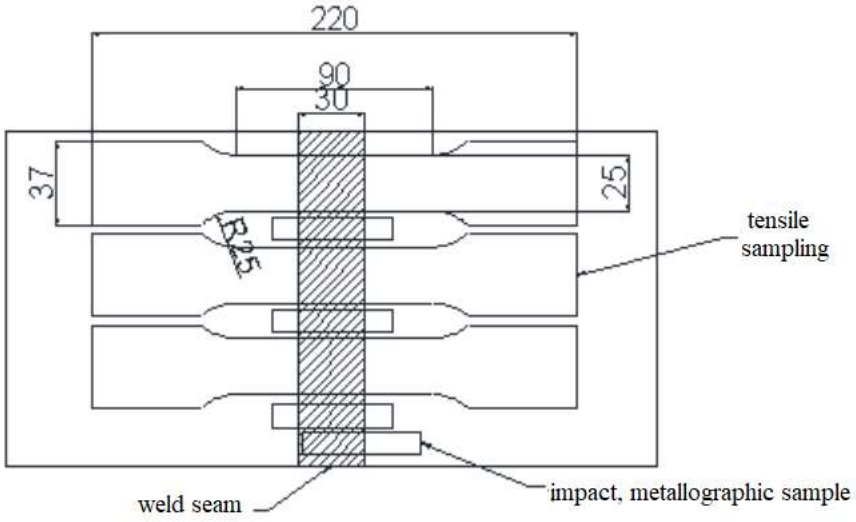

Fig.2 Sampling diagram of samples

ISSN: 2414-1895 DOI: 10.6919/ICJE.202405_10(5).0023

The tensile samples (as illurstrated in Fig.2) were prepared in accordance with the relevant provisions in the standard GB/T2651-2008. The welding zone is located in the middle of the tensile sample. The test was carried out on a universal tensile testing machine (SHT4305) at room temperature. The recorded data was the average value of four tensile samples.

The impact performance tests used V-type standard notch impact samples in accordance with the requirements of standard GB/T2650-2008. The tests were carried out by using a pendulum impact testing machine (PTM2302) at room temperature (about 22 ℃). The recorded data took the average value of three samples.

3. Results and Analysis

3.1 Macro and Microstructure of Welded Joint

The appearance inspection of the welded joint was carried out according to the standard NB/T 47014-2011. The weld seam of the welded joint was beautifully formed. No defects of non-penetrating weld, incomplete fusion, pore, sticky slag and crack were observed, as shown in Fig.3. The deformation of the welded joints of each group's samples is small. It suggests that the welded joints obtained by the welding parameters set in this study can meet the requirements of standard.

(a)2# weld seam of welded joint (b)2# section of welded joint

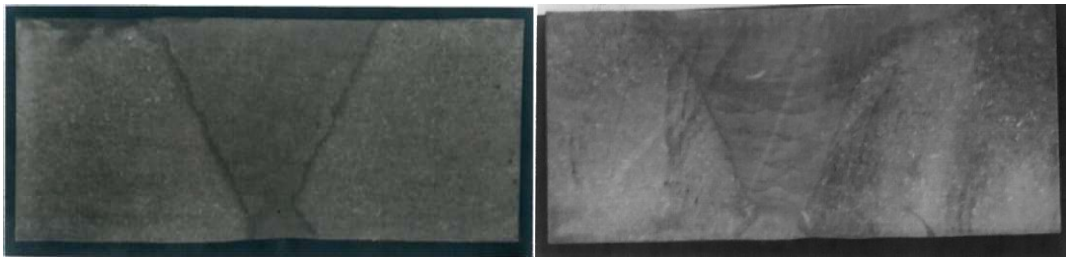

(c) sample 2 # cross section of joint (d) sample 3 # cross section of joint

Fig.3 Macro morphology of the welded joints

The microstructure analysis was carried out on the weld seam metal of welded joint according to the standard GB/T 13298-2015 by using an OLYMPUS GX-71F metallurgical microscope. The observed microstructure is shown in Fig.4. The welding zone was mainly composed of lath martensite. A small amount of δ ferrite formed due to the existence of composition gradient. The starting time of the martensite phase transformation was different. The martensite lath was generated in sequence in the same austenite grain, the directions of lath were different and were divided into several lath zones. When the martensitic lath rise, the collision between lath increases the dislocation density [4-5].

ISSN: 2414-1895 DOI: 10.6919/ICJE.202405_10(5).0023

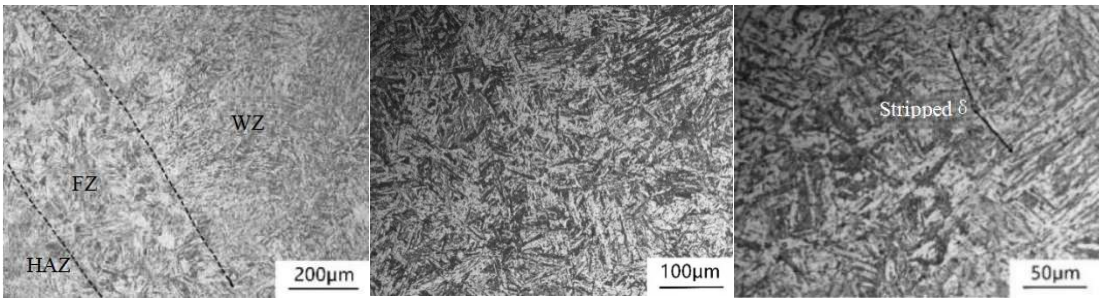

(a)1#sample1 fusion zone (a)1#sample2 weld seam zone (a) 1#sample3 weld seam zone

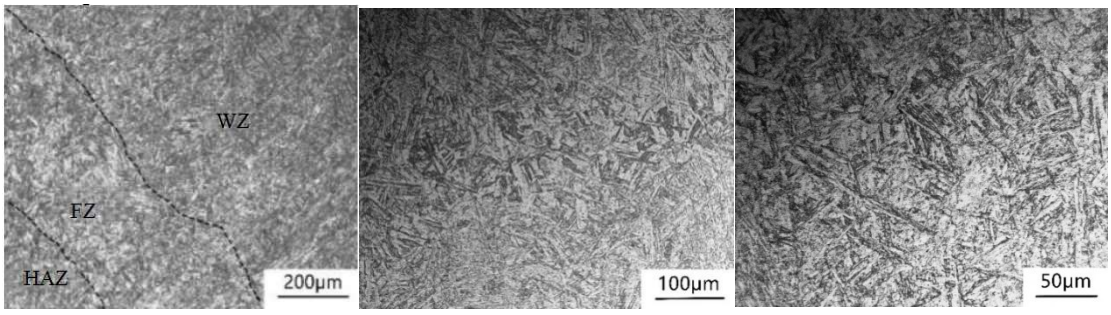

(b)2#sample1 fusion zone (b)2#sample2 weld seam zone (b) 2#sample3 weld seam zone

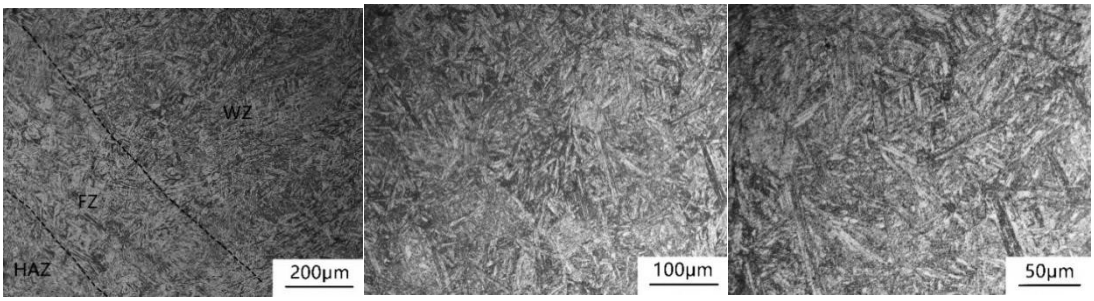

(c)3#sample1 fusion zone (c)3#sample2 weld seam zone (c) 3#sample3 weld seam zone

Fig.4 Microstructure characteristics of weld seam at different interlayer temperatures (a: 140℃ \ b170℃ \ c200℃)

During the multilayer multi-pass welding, the latter welding processes can be regarded as the post-welding heat treatment of the previous weld. So, the higher the interlayer temperature, the slower the cooling rate. Therefore, the crystal grain size become larger, and the obtained martensite microstructure is also coarser [6]. Under the condition of this test, the line energy is the same. The microstructure of the welding zone at different interlayer temperatures does not differ much, and it is also dominantly composed of lath martensite microstructure, containing a small amount of δ ferrite. However, as the interlayer temperature of weld seam rises, the width of lath in the lath martensite microstructure in the weld zone slightly grows, as shown in Fig. 4(a)3, (b)3, (c)3.

As can be seen in Fig.5, the diffraction peaks in the XRD patterns of the heat-affected zone and weld seam zone of the welded joints are mainly martensite. Also, austenite diffraction peak with a relatively lower intensity is detected. The higher the interlayer temperature of the weld seam, the higher the austenite diffraction peak in the weld zone. This may be explained that the cooling speed in the weld zone is relatively slow, thus the alloy elements will accumulate in the final-solidification area, forming a small amount of austenite.

ISSN: 2414-1895 DOI: 10.6919/ICJE.202405_10(5).0023

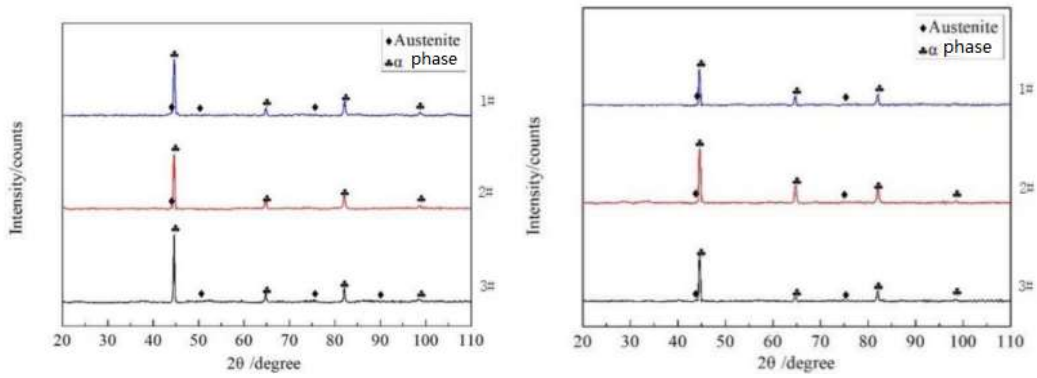

(a) the XRD patterns of heat affected zone in samples 1 #, 2 #, and 3#; (b) sample 1 #, 2 #, and 3# XRD pattern of weld seam zone

Fig.5 The XRD patterns of the heat affected zone and weld bzead one

3.2 Mechanical Properties of Welded Joint

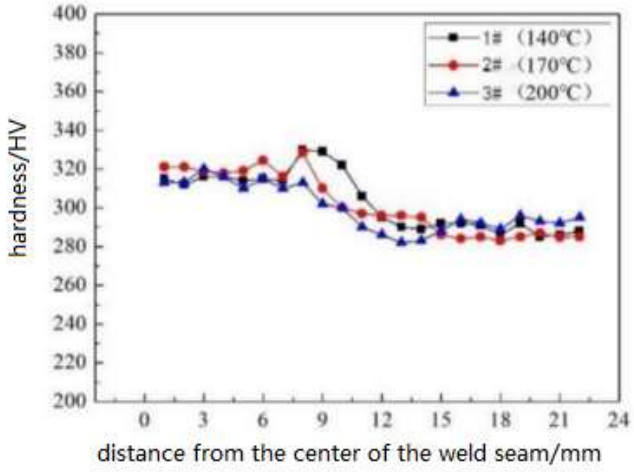

Fig.6 Relationship between the interlayer temperature and microhardness in the weld.

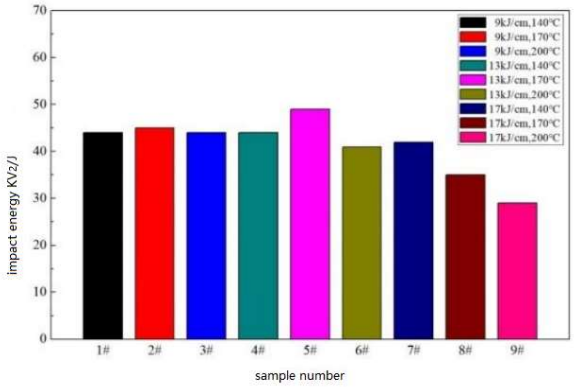

Fig.7 Impact absorption energy of the weld seam zone under different welding processes

The effect of interlayer temperature on the microhardness of welded joints is shown in Fig.6. It shows that the influence of interlayer temperature on the hardness of the weld seam zone is relatively small under the test condition of this study. The hardness of the weld seam zone ranges between 315HV-325HV. The slight fluctuation of the data could be considered as a result of systematic error of experiments. This is related to the three-interlayer temperature (140℃, 170℃, 200℃) weld seam

ISSN: 2414-1895 DOI: 10.6919/ICJE.202405_10(5).0023

zone which are based on lath martensite, containing a small amount of δ ferrite and a small amount of austenite.

Fig.7 further shows the influences of welding line energy and interlayer temperature on the impact performance. When the interlayer temperature was 140℃, the impact energy absorbed in the weld seam zone gradually reduced with the increase of line energy (from 9 kJ/cm to 17 kJ/cm). The impact energy absorbed of weld seam was 42 J when the line energy is 9 kJ/cm. When the interlayer temperature was 170℃, with the increase of line energy, the impact energy absorbed of the weld seam zone increased first and then decreased. The highest impact energy of 49 J was obtained when the line energy was 13 kJ/cm. As the interlayer temperature increased up to 200°C, the impact energy absorbed in the weld seam zone decreased as the line energy increased. The lowest work absorbed in the weld seam zone was obtained to be 29 J with a line energy of 17 kJ/cm. Here, both the energy of the weld line and the interlayer temperature were the highest. The high temperature residence time was prolonged, which slowed down the cooling rate. Therefore, the grains grew more significantly, leading to a coarse martensitic microstructure and more δ ferrite [6]. As a result, the impact toughness of the weld seam zone was the worst.

The tensile properties of the welded joints under the line energy of 13 kJ/cm are shown in Table 5. Under all various welding process parameters, the tensile strength of welded joint Rm is higher than 812MPa (all values are higher than the standard: Rm ≥ 780MPa) and the yield strength RP0.2 is larger than 630MPa. These values are higher than the base material. The elongation A is larger than 16.0%. In addition, the influence of interlayer temperature on the strength performance and elongation (plasticity) of the welded joints is not significant. This is most likely due to the moderate line of 13 kJ/cm and the subsequently formed ideal microstructure. The main reason for the higher strength of welded joints compared to that of the base material may be that the Cr, Mo, and Ni atoms substitute the Fe atoms in the weld seam at high temperature, forming a substitutional solid solution. This then caused lattice distortion, hindering the dislocation movement, and thus enhanced the strength of metal at the weld seam [6].

Table 5. Tensile test results of welded joints with different welding parameters.

sample number	yield strength $R_{P0.2}$/MPa	tensile strength R_m/MPa	elongationA/%	fracture position
1#	634.7	812.7	16.5	base material
2#	638	812.5	16.7	base material
3#	636.7	812.1	16.3	base material

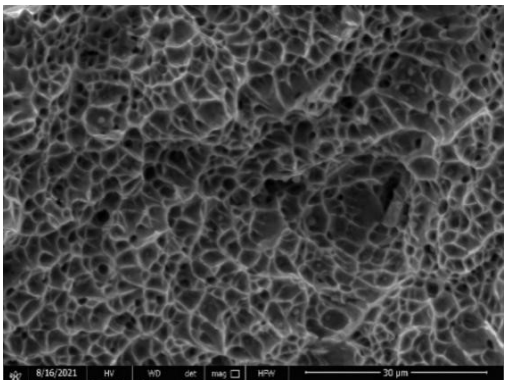

Fig.8 Impact fracture morphology of the welded joint 2 #

ISSN: 2414-1895 DOI: 10.6919/ICJE.202405_10(5).0023

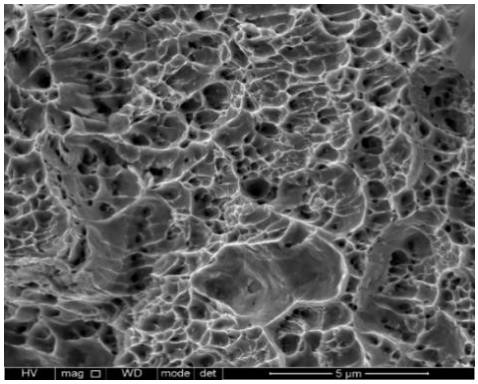

Fig.9 Tensile fracture morphology of the welded joint 2 #

Fig.8 and Fig.9 are the impact fracture morphology and the tensile fracture morphology of welded joints 2#, respectively. It is observed that both the impact fracture and tensile fracture produced typical equiaxed dimples. Comparatively, the size of dimples caused by the impact fracture is more uniform compared to that of tensile fracture. It is suggested that the dimple morphologies is related to a martensite microstructure weld seam.

4. Conclusion

(1) Good quality weld seam of welded joint is formed without defects of non-penetrating weld, incomplete fusion, pore, sticky slag, and crack.

(2) The impact of interlayer temperature on weld seam microstructure is negligible. Under the same line energy, the formed microstructures of the weld seam zone at different interlayer temperatures is similar, all of which are composed of dominantly lath martensite microstructure, and a small amount of δ ferrite.

(3) The weld seam zone exhibited the highest strength, toughness, and plasticity as well as the best impact energy at the interlayer temperature of 170℃ with a line energy of 13 kJ/cm.

Acknowledgments

Project supported by Science and Technology Support Project of Sichuan Province (20ZDZX0042).

References

[1] Luo Xingqi, Zhu Guojun, Feng Jianjun. Progress and Development Trends in Hydraulic Turbine Technology [J]. Journal of Hydroelectric Engineering, 2020,39 (08): 1-18.

[2] Yang Hang, Zhu Xin, You Kai. Analysis on Welding Technology of Left Bank Volute of Baihetan Hydropower Station [J]. Yangtze River, 2020,51 (S2): 138-142.

[3] Zhang Ran, Kang Jinwu, Huang Tianyou, et al. Experimental Study and Application of the Martensitic Transformation Plasticity of ZG0Cr13Ni5Mo Stainless Steel [J]. Journal of Tsinghua University (Science and Technology), 2010,50 (08): 1183-1187.

[4] Liu Yixiang, Wu Jingzi. Composition and Microstructure in the Fusion Zone of Cladding Welding [J]. Physical Testing and Chemical Analysis(Part A:Physical Testing), 1999 (01): 9-11+34.

[5] Luo Changshen, Guo Yi. Microstructure and Mechanical Property of 1Cr13 Martensitic Stainless Steel Welded with 00Cr13Ni5Mo Welding Wire [J]. Hot Working Technology, 2011, 40 (03): 143-146.

[6] Liu Tiegang, Wu Yidang, Wang Defu, et al. Effect of Interpass Temperature on Impact Toughness of 18mnd5 Steel Welded Joint for Nuclear Power [J]. Electric Welding Machine, 2020,50 (06): 79-83.

[7] Liu Xianwen. The Welding Process, Microstructure and Properties of S32101 Duplex Stainless Steel [D]. Xi'an University of Technology, 2017.